GEOPHYSICAL RESEARCH LETTERS, VOL. ???, XXXX, DOI:10.1002/,

Tropical Climate Change Control of the Lower Stratospheric Circulation

Pu Lin,[1] Yi Ming,[2] and V. Ramaswamy[2]

Corresponding author: Pu Lin, Program in Atmospheric and Oceanic Sciences, Princeton University, 300 Forrestal Road, Princeton, NJ 08544, USA. (Pu.Lin@noaa.gov)

[1]Program in Atmospheric and Oceanic Sciences, Princeton University, Princeton, NJ, USA.

[2]Geophysical Fluid Dynamics Laboratory/NOAA, Princeton, NJ, USA.

The behavior of the Brewer-Dobson circulation is investigated using a suite of global climate model simulations with different forcing agents, in conjunction with observation-based analysis. We find that the variations in the Brewer-Dobson circulation are strongly correlated with those in the tropical-mean surface temperature through changes in the upper tropospheric temperature and zonal winds. This correlation is seen on both interannual and multi-decadal timescales, and holds for natural and forced variations alike. The circulation change is relatively insensitive to the spatial pattern of the forcings. Consistent changes in the Brewer-Dobson circulation with respect to those in the tropical-mean surface temperature prevail across timescales and forcings, and constitute an important attribution element of the atmospheric adjustment to global climate change.

1. Introduction

The Brewer-Dobson circulation (BDC) is a major feature of the Earth's climate system, consisting of the slow overturning motion of the stratosphere, with ascent in the tropics and descent in the extratropics [*Holton et al.*, 1995; *Randel and Jensen*, 2013; *Butchart*, 2014]. This airflow determines the meridional thermal structure of the stratosphere, and impacts the transport and distribution of important climate-influencing constituents in the lower stratosphere including water vapor, volcanic aerosols and ozone [*Randel and Jensen*, 2013; *Butchart*, 2014]. Recent studies suggested that the stratosphere-troposphere dynamical coupling could be a source of climate predictability [*Thompson et al.*, 2002; *Cohen et al.*, 2007], and changes in the aforementioned stratospheric species may have significantly altered the climate over the past few decades [*Solomon et al.*, 2010; *Dessler et al.*, 2013; *Robock*, 2000; *Forster and Shine*, 1997; *Polvani et al.*, 2011]. It is therefore essential to understand how the BDC would behave in response to anthropogenic climate forcings and in the context of natural variability.

Previous modeling studies identified a long-term strengthening trend of the BDC as a result of greenhouse gases (GHGs)-induced warming [*Butchart et al.*, 2010; *Butchart*, 2014]. The strengthening is more pronounced for its shallow branch (below 30 hPa) [*Lin and Fu*, 2013]. Yet, the BDC responses to other forcing agents such as anthropogenic aerosols and major volcanic eruptions have not been investigated fully with very few exceptions [*Tilmes et al.*, 2009]. On interannual timescales, observations and simulations indicated a more vigorous BDC in the lower stratosphere during the warm phase of the El Niño-Southern Oscillation (ENSO) [*Randel et al.*, 2009; *Calvo et al.*, 2010; *Simpson et al.*, 2011]. In this study, we show that the close linkage between the BDC shallow branch and tropical-mean surface temperature (TT) is not unique to ENSO or GHG forcing, and may be applicable to other timescales and externally forced components.

2. Data and Method

We make use of the simulations conducted with the NOAA/Geophysical Fluid Dynamics Laboratory (GFDL) global climate model CM3 [*Donner et al.*, 2011]. The GFDL CM3 model is a fully coupled atmosphere-ocean climate model with a model top at 0.01 hPa ($\sim$ 86 km). It has 48 vertical layers, of which 25 layers are located above 100 hPa, and a horizontal resolution of $\sim$ 200 km. Its tropospheric and stratospheric chemistry scheme is fully interactive. It also implements an explicit treatment of aerosol-cloud interaction [*Ming et al.*, 2006, 2007]. CM3 is one of the Coupled Model Intercomparison Project phase 5 (CMIP5) models in support of the Intergovernmental Panel on Climate Change (IPCC) Fifth Assessment Report. The atmospheric component of CM3 with simpler tropospheric chemistry takes part in the second Chemistry Climate Model Validation Activity (CCMVal-2), which forms the basis of the recent scientific assessment of ozone depletion conducted by the World Meteorological Organization (WMO) and the United Nations Environment Programme (UNEP) [*WMO*, 2011], and performs as well as or better than its peers in many aspects [*SPARC CCMVal*, 2010].

We analyze a 1700-year control simulation in which all forcings are fixed at the 1860 (pre-industrial) levels, and a suite of historical simulations forced with different forcing combinations. These historical simulations include: all forcing runs (AllForc), natural forcing runs (Natural), anthropogenic forcing runs (Anthro), anthropogenic aerosol forcing only runs (Aerosol), and greenhouse gases and stratospheric ozone only runs (WMGGO3). These historical experiments are configured following the Coupled Model Intercomparison Project Phase 5 (CMIP5) guidelines [*Taylor et al.*, 2012]. Each historical experiment consists of three ensemble members and covers 1860-2004. In our analysis, each member is treated as an independent sample. More details of this model and simulations can be found in *Donner et al.* [2011] and *Austin et al.* [2013].

We also examine the simulations conducted with CM2.1, an earlier generation GFDL coupled model [*Delworth et al.*, 2006]. It is one of the CMIP3 models used for the IPCC Fourth Assessment Report. It has 24 levels in the atmosphere with a model top at 3 hPa ($\sim$ 40km). Its horizontal resolution is $\sim$ 200 km. CM2.1 does not include interactive chemistry in the stratosphere, and the stratospheric ozone concentration is prescribed. Nor does it consider aerosol-cloud interactions. We analyze the CM2.1 historical simulations (1861-2000) in three experiments: Natural, Aerosol and WMGGO3. Each experiment consists of three ensemble members.

We analyze the ERA-interim reanalysis data for 1979-2012 [*Dee et al.*, 2011]. The Transformed Eulerian Mean (TEM) velocity from the ERA-interim reanalysis is calculated using 6-hourly data following its definition [*Andrews et al.*, 1987]. *Seviour et al.* [2012] found that the climatology of the BDC is well represented in this reanalysis dataset. The reanalysis data is compared with simulations by the atmospheric component of CM3 (namely AM3) driven by the observed sea surface temperatures (SSTs) and all forcing agents.

The strength of the BDC is commonly represented by the mass flux calculated from the TEM velocity [*Andrews et al.*, 1987, see appendix for the calculation of the mass flux]. We define the shallow branch of the BDC as the upward mass flux across 70 hPa but not reaching 30 hPa, and the deep branch as the mass flux that rises above 30 hPa [*Lin and Fu*, 2013]. We compute the time series of annual mean mass fluxes transported by the shallow and the deep branch of the BDC, as well as annual mean surface temperature averaged over $20°S - 20°N$.

3. Results

We first examine the BDC in the CM3 control simulation. Figure 1 shows the squared coherence between the strength of the BDC and TT, which measures the correlation between the two time series at different frequencies. The BDC shallow branch shows strong correlations with TT at all frequencies, while the coherence between the BDC deep branch and TT is much lower. No appreciable phase difference is found between the BDC shallow branch and TT (not shown).

We then analyze the CM3 historical simulations driven by different combinations of forcing agents. Note that this coherence/phase analysis would require a long time series or a large number of ensembles to resolve the full spectrum, and hence it is not suitable for historical simulations or reanalysis products. We therefore focus on variations of two timescales in the following text. The deviations from five-year running means provide a measure of interannual variations, and the averages of consecutive (non-overlapping) five-year segments are used to describe variations on decadal to multi-decadal timescales. Correlation coefficients are calculated between the BDC and TT on these two timescales and summarized in Table 1. Strong correlations are found between the BDC shallow branch and TT on both timescales in all experiments.

On the interannual timescale, the variations in TT is dominated by ENSO with a distinct spatial structure over the central and eastern Pacific, but ENSO may not be the only contributor to the correlation between TT and the BDC shallow branch. We select ENSO-neutral years as those in which the magnitude of the annual mean Nino3.4 index [*Trenberth and Stepaniak*, 2001] is less than 0.2°C. This subset of ENSO-neutral years exhibits similar relationship between the BDC and TT (Fig. 2(a) and Table 1), indicating non-ENSO processes underlying interannual variability behave in a manner similar to ENSO. The correlations between the BDC and TT on the interannual timescale in the forced simulations are similar to those in the unforced control simulations. This is not surprising given that most of the interannual variations are internally generated.

On the decadal to multi-decadal timescales, external forcing agents give rise to variations that are often larger than the internal (unforced) ones. In particular, major volcanic eruptions cause a cooling of the subsequent few years at the surface, while anthropogenic GHGs (aerosols) give rise to a secular warming (cooling) trend, which is most appreciable over the second half of the 20th century. The volcanic aerosols also heat the lower stratosphere radiatively, while GHGs cool the stratosphere, and anthropogenic aerosols have little radiative effect on the stratosphere. Despite these different temporal and spatial variations, the forced simulations invariantly show the strength of the BDC shallow branch being strongly correlated with TT as shown in Fig. 2(b).

To shed light on the robustness of the CM3 results with regards to model formulation, we repeat the same analysis for CM2.1. As shown in Table 1, the correlation between the BDC shallow branch and TT in CM2.1 largely resemble those in CM3. But the magnitudes of the changes in the shallow branch in CM2 is weaker than those in CM3 (not shown) for reasons detailed in the next section.

In addition to model simulations, we also examine the ERA-interim reanalysis data (1979-2012) for possible observational evidence. Due to the relatively short time span of the reanalysis data, we only analyze the interannual variations as shown in Fig. 3. For further comparison, we also present the results based on the three-member ensemble simulated with AM3, which is driven by the observed SSTs and all forcing agents. Note that the Quasi-Biennial Oscillation (QBO), though absent in the model simulations, can modulate the strength of the BDC in the real world (and reanalysis) [*Holton and Tan*, 1980], thus giving rise to interannual variations that are independent of TT. For a cleaner comparison with model simulations, we remove the QBO signal in the monthly mass flux from reanalysis by regressing upon a pair of QBO indices [*Randel and Wu*, 1996]. As shown in the figure, the reanalysis gives a very similar result to the AM3 simulations. Without removing the QBO signal in the reanalysis data, the correlation coefficient between TT and the BDC shallow branch would be lower ($r = 0.56$).

The correlation coefficients between the BDC deep branch and TT are always lower than those between the shallow branch and TT (Table 1), and the responses in the BDC deep branch to changes in TT are generally weaker (Fig. S1 vs. Fig. 2). The correlation between the BDC deep branch and TT is stronger in CM2.1 than in CM3. The difference between these two models will be discussed in the next section.

4. Discussion

The influence of TT on the BDC shallow branch is realized through modulating zonal wind structures in the upper troposphere/lower stratosphere (UTLS). This is because the BDC is driven by the dissipation of Rossby waves and gravity waves in the stratosphere [*Holton et al.*, 1995; *Butchart*, 2014], and the propagation and dissipation of these waves are modulated by zonal wind structures [*Andrews et al.*, 1987]. As the tropical surface warms, stronger zonal winds are seen in the subtropical UTLS (Fig. S2 (a), (b) and Fig. S5). This leads to an upward shift of the critical layer, where wave dissipation preferentially occurs [*Randel and Held*, 1991], and hence stronger wave dissipation in the lower stratosphere (Fig. S2 (c), (d) and Fig. S6). This stronger wave dissipation then drives a stronger BDC. This critical layer control mechanism has been invoked to explain the strengthening of the BDC caused by GHGs [*Garcia and Randel*, 2008; *Shepherd and McLandress*, 2011] and during the warm phase of ENSO (El Niño) [*Calvo et al.*, 2010]. The reanalysis data provides further observational evidence (Fig. S3).

The zonal wind changes in the subtropical UTLS largely result from changes in the tropics-to-mid-latitudes temperature gradient following the thermal wind balance. Owing to moist convection, the tropical surface and free troposphere temperatures are tightly coupled in the sense that the vertical temperature gradient follows approximately the moist adiabatic lapse rate. As a result, when TT varies, greater temperature changes are seen aloft. The largest temperature responses are seen around 200 hPa in the tropics, roughly doubling those at the surface (Fig. S2). Note that the 200 hPa level corresponds to the tropopause over mid-latitudes, where temperature does not vary much with that at the surface (Fig. S4). Thus a warmer surface would lead to a strong increase of the tropics-to-mid-latitudes temperature gradient at this tropical UT/mid-latitude LS region. During El Niño events, the narrowing of the tropical belt introduces additional meridional temperature gradients throughout the troposphere by modulating the transient eddy momentum flux [*Seager et al.*, 2003; *L'Heureux and Thompson*, 2006].

The strengthened BDC following a warmer surface, in turn, cools the tropics and warms the extratropics in the stratosphere through the anomalous vertical motion. The colder tropics and warmer extratropics above 100 hPa help to confine the zonal wind anomalies within the lower stratosphere. Therefore, the wave dissipation at middle/upper stratosphere and the BDC deep branch are relatively insensitive to changes in TT. In addition, the radiative effect of GHGs, ozone and volcanic aerosols in the stratosphere could further modify the temperature gradient and zonal wind structure there.

Previous studies have discussed the different responses in the zonal mean circulation to El Niño, greenhouse gases and aerosols, especially in the context of the Hadley circulation [*Lu et al.*, 2008; *Ming and Ramaswamy*, 2011]. Our results, however, suggest a consistent response in the BDC shallow branch with respect to changes in the tropical-mean surface temperature regardless of the imposed forcings. The spatial distribution of the forcing and the detailed surface temperature patterns, which lead to diverse responses in the Hadley circulation, remain secondary in this regard. Indeed, we see similar temperature and zonal wind patterns in the UTLS region in response to changes in TT on different timescales and under different forcings, despite very different responses at the surface and in the middle/upper stratosphere (Fig. S4, S5, S6). Following these similar UTLS temperature and zonal wind changes is a similar response in the BDC shallow branch among different forcings (Fig. 2(b)).

To further illustrate the insensitivity of the BDC to the spatial pattern of the surface temperature, we perform an atmosphere-only model experiment in which SST is uniformly increased by 4K while keeping all forcing agents constant. The resulting UTLS temperature and zonal wind changes agree well with the decadal-to-multi-decadal variations under different forcings (Fig. S5 and S6). The strengthening of the BDC shallow branch per unit surface warming in this idealized experiment also matches those seen for different forcings (Fig. 2).

In this chain of events linking changes in TT and the BDC, the vertical amplification of temperature in the tropics plays an important role as it determines the meridional temperature gradient in the subtropical UTLS. While it is a robust feature seen in observations and model simulations [*Fu and Johanson*, 2005; *Ramaswamy et al.*, 2006], the magnitudes of the vertical amplification varies from model to model, and models generally overestimate the amplification when compared with available observations [*Fu et al.*, 2011; *Po-Chedley and Fu*, 2012]. This difference in the temperature response in the tropical upper troposphere is evidently factored in the BDC response. *Lin and Fu* [2013] compared the trends in the BDC over the 21st century simulated by a group of chemistry climate models with identical external forcing and similar SSTs. They found that the models with stronger warming in the tropical upper troposphere also simulate stronger acceleration of the BDC (see their Figs. 11 and 12). Note that this study does not address to what extent the discrepancy in the upper tropospheric warming among models is caused by that in the surface warming or by that in the free trpospheric amplification.

For the two models employed here, CM3 shows a stronger vertical amplification than CM2.1, presumably due to the difference in the cumulus parameterization. The BDC shallow branch strengthening per unit surface warming in CM3 is also larger than in CM2.1, a finding that is consistent with *Lin and Fu* [2013]. Furthermore, CM2.1 has a weaker climatological BDC shallow branch and less wave dissipation in the lower stratosphere than CM3. Thus one would expect fewer changes in the wave dissipation following the shift of the critical layer, rendering the BDC shallow branch less sensitive to changes in the subtropical jets. This weaker response in the BDC shallow branch in CM2.1 may be related to its stronger response in the deep branch, as the weaker temperature gradient in the lower stratosphere would allow the subtropical wind anomalies to penetrate deeper into the stratosphere.

5. Summary and Implication

We present a robust correlation between the BDC shallow branch and TT that is seen on a range of timescales from interannual to multi-decadal and for natural and forced variations alike. Within a particular model (and possibly in the real world), the lower stratopsheric circulation shows consistent changes with respect in TT for different external forcings. This invariant influence of changes in the tropical-mean surface temperature upon the lower stratospheric circulation is realized through the strong and robust changes in the temperature and zonal wind structures in the subtropical UTLS. Therefore, the variations in the BDC on a wide range of timescales can be perceived simply as responsive to changes in the atmospheric zonal-mean thermal and wind structures that follow, at least to the first order, changes in the tropical-mean surface temperature without knowing details of the forcings that drive these changes. Note that while the radiative forcings cannot be directly measured and hence bear persistent uncertainties in the magnitudes and spatial distributions, observations of the surface temperature are much more feasible and reliable, and model simulations of the surface temperature are relatively well constrained. Given the robustness of the underlying physical mechanism, we can gain more confidence in the climate model projection of the long-term trends of the stratospheric circulation, composition and its downward impacts on the troposphere and surface by comparing with the short-term observations. On the other hand, one would expect different response in the stratospheric circulation to changes in the tropical-mean surface temperature for different models and observations, in light of their discrepancies in the tropical upper tropospheric temperature change. Further investigation is needed to reconcile this uncertainty among models and observations.

Appendix A: Diagnosis of the BDC in model simulations

Because the BDC is a very slow Lagrangian circulation, direct measurement of its strength is difficult. It is commonly approximated by the diabatic circulation (which dynamically balances the diabatic heating in the meridional plane), or the residual circulation represented by the Transformed Eulerian Mean (TEM) stream function Ψ^* [*Andrews et al.*, 1987]. The strength of the BDC is then represented by the mass flux transported by the TEM velocity. The TEM velocity can be calculated following its definition [*An-*

drews et al., 1987; *Hardiman et al.*, 2010] or the "downward control principle" [*Haynes et al.*, 1991], both of which inconveniently require knowledge of high frequency data (four times daily or higher). In this study, we diagnose TEM velocity by solving the TEM thermodynamic equation, a method requiring only monthly data.

The TEM thermodynamic equation is:

$$\bar{\theta}_t - (a\rho_0 cos\phi)^{-1}\Psi^*_z\bar{\theta}_\phi + (a\rho_0 cos\phi)^{-1}\Psi^*_\phi\bar{\theta}_z - \bar{Q} = -\rho_0^{-1}[\rho_0(\overline{v'\theta'}\bar{\theta}_\phi/a\bar{\theta}_z + \overline{w'\theta'})]_z \quad \text{(A1)}$$

in which overbars denote zonal means, primes denote deviation from zonal means, and subscripts denote derivatives. Q is the diabatic heating rate, and other variables follow their conventional definitions. The right-hand side of the above equation is usually small and omitted, and all variables on the left-hand side except Ψ^* can be read from monthly mean model outputs. A straightforward integration of this equation is not possible due to numerical instabilities. Previous studies employed iterative methods to solve this equation [*Solomon et al.*, 1986; *Rosenlof*, 1995], which do not guarantee the convergence to the solution. Following *Santee and Crisp* [1995], we first take the derivative of the entire equation with respect to ϕ. The resulting equation can be easily solved using the finite differential method with the boundary condition $\Psi^* = 0$ at poles. Mass flux is calculated from monthly Ψ^* and then averaged annually.

We further diagnose wave forcing X from the TEM momentum equation:

$$\bar{u}_t - (\rho_0 cos\phi)^{-1}\Psi^*_z[(acos\phi)^{-1}(\bar{u}cos\phi)_\phi - f] + (\rho_0 acos\phi)^{-1}\Psi^*_\phi\bar{u}_z = X \quad \text{(A2)}$$

The dissipation of Rossby waves in the stratosphere deposits easterly momentum and decelerates the mean flow there. Stronger wave dissipation is indicated by a more negative

X and would lead to a stronger BDC. Note that X includes the contributions from both resolved and subgrid waves, and is equivalent to the divergence of the Elassen-Palm (EP) flux for resolved waves [*Andrews et al.*, 1987].

Appendix B: Calculation of the cross-spectrum

The coherence and the phase of two time seriese are estimated from the cross spectrum analysis [*von Storch and Zwiers*, 1999]. The squared coherence between two time series x and y is:

$$Coh^2 = |\overline{F_{xy}}|^2/(\overline{P_x P_y}) \tag{B1}$$

in which F_{xy} is the cross-spectrum density between x and y, P_x and P_y are the power spectra of x and y, respectively. The overbar represents averaging over segments. The 1700 year timeseries is divided into 105 segments, each consists of 32 years and overlaps by 16 years with the adjecent segments. The last 4 years are discarded. Each segment is weighted with the Hamming window and zero-padded to form a 256-year-segment, and the spectrum is estimated using Welch's method for each segment with a bandwith of 1/256 cycle per year. The degree of freedom for the spectral estimeates is $n = f_\omega N/M_{sp}$, $N = 1700$ is the total sample size, $M_{sp} = 128$ is the number of spectral estimates, and $f_\omega \approx 1.3$ is the factor used to compensate for smoothing done by the Hamming window. This give a degree of freedom $n \approx 17$. The 95% confidence interval for a zero squared coherence is $1 - 0.05^{1/(n-1)} \approx 0.17$ [*Emery and Thomson*, 2001].

Acknowledgments. The model simulation used in this paper is available at NOAA/GFDL's data portal. European Centre for Medium-Range Weather Forecasts

(ECMWF) ERA4-Interim data used in this study have been obtained from the ECMWF data server. We thank Drs. Isaac Held and R. John Wilson for reviewing an earlier version of this manuscript. This paper was prepared by Pu Lin under award NA08OAR4320752 from the National Oceanic and Atmospheric Administration, U.S. Department of Commerce. The statements, findings, conclusions, and recommendations are those of the author(s) and do not necessarily reflect the views of the National Oceanic and Atmospheric Administration, or the U.S. Department of Commerce.

References

Andrews, D. G., J. R. Holton, and C. B. Leovy (1987), *Middle Atmosphere Dynamics*, *International Geophysical Series*, vol. 40, 489 pp., Academic Press, San Diego.

Austin, J., L. W. Horowitz, M. D. Schwarzkopf, R. J. Wilson, and H. Levy II (2013), Stratospheric ozone and temperature simulated from the preindustrial era to the present day, *J. Clim.*, *26*, 3528–3543.

Butchart, N. (2014), The Brewer-Dobson circulation, *Rev. Geophys.*, *52*, 157–184.

Butchart, N., et al. (2010), Chemistry-climate model simulations of twenty-first century stratospheric climate and circulation changes, *J. Clim.*, *23*, 5349–5374, doi: 10.1175/2010JCLI3404.1.

Calvo, N., R. R. Garcia, W. J. Randel, and D. R. Marsh (2010), Dynamical mechanism for the increase in tropical upwelling in the lowermost tropical stratosphere during warm ENSO events, *J. Atmos. Sci.*, *67*, 2331–2340.

Cohen, J., M. Barlow, P. J. Kushner, and K. Saito (2007), Stratosphere-troposphere coupling and links with Euraisan land surface variability, *J. Clim.*, *20*, 5335–5343.

Dee, D. P., et al. (2011), The ERA-Interim reanalysis: configuration and performance of the data assimilation system, *Q. J. Roy. Meteorol. Soc.*, *137*, 553–597, doi: 10.1002/qj.828.

Delworth, T. L., et al. (2006), GFDL's CM2 global coupled climate models. Part I: Formulation and simulation characteristics, *J. Clim.*, *19*, 643–674.

Dessler, A. E., M. R. Schoeberl, T. Wang, S. M. Davis, and K. H. Rosenlof (2013), Stratospheric water vapor feedback, *Proc. Natl. Acad. Sci. (USA)*, doi: 10.1073/pnas.1310344110.

Donner, L. J., et al. (2011), The dynamical core, physical parameterizations, and basic simulation characteristics of the atmospheric component AM3 of the GFDL Global Coupled Model CM3, *J. Clim.*, *24*, 3484–3519.

Emery, W. J., and R. E. Thomson (2001), *Data Analysis Methods in Physical Oceanography: Second and Revised Edition*, 638 pp., Elsevier, New York.

Forster, P. M. D., and K. P. Shine (1997), Radiative forcing and temperature trends from stratospheric ozone changes, *J. Geophys. Res.*, *102*, 10,841–10,855, doi: 10.1029/96JD03510.

Fu, Q., and C. M. Johanson (2005), Satellite-derived vertical dependence of tropical tropospheric temperature trends, *Geophys. Res. Lett.*, *32*, L10703, doi: 10.1029/2004GL022266.

Fu, Q., S. Manabe, and S. M. Johanson (2011), On the tropical upper tropospheric warming: models versus observations, *Geophys. Res. Lett.*, *38*, L15704, doi: 10.1029/2011GL048101.

Garcia, R. R., and W. J. Randel (2008), Acceleration of the Brewer-Dobson circulatio due to increase in greenhouse gases, *J. Atmos. Sci.*, *65*, 2731–2739, doi: 10.2275/2008JAS2712.1.

Hardiman, S. C., D. G. Andrews, A. A. White, N. Butchart, and I. Edmond (2010), Using different formulations of the transformed Eulerian-mean equations and Eliassen-Palm diagnostics in general circulation models, *J. Atmos. Sci.*, pp. 1983–1995.

Haynes, P. H., C. J. Marks, M. E. McIntyre, T. G. Shepherd, and K. P. Shine (1991), On the downward control of extratropical diabatic circulations by eddy-induced mean zonal forces, *J. Atmos. Sci.*, *48*, 651–679.

Holton, J. R., and H.-C. Tan (1980), The influence of the equatorial quasi-biennial oscillation on the global circulation at 50 mb, *J. Atmos. Sci.*, *37*, 2200–2208.

Holton, J. R., P. H. Haynes, M. E. McIntyre, A. R. Douglass, R. B. Rood, and L. Pfister (1995), Stratosphere-troposphere exchange, *Rev. Geophys.*, *33*, 403–439, doi: 10.1029/95RG02097.

L'Heureux, M. L., and D. W. J. Thompson (2006), Observed relationships between the El Niño-Southern Oscillation and the extratropical zonal-mean circulation, *J. Clim.*, *19*, 276–287.

Lin, P., and Q. Fu (2013), Changes in various branches of the Brewer-Dobson circulation from an ensemble of chemistry climate models, *J. Geophys. Res.*, *118*, 73–84, doi:10.1029/2012JD018813.

Lu, J., G. Chen, and D. M. W. Frierson (2008), Response of the zonal mean atmospheric circulation to El Niño versus global warming, *J. Clim.*, *21*, 58355,851.

Ming, Y., and V. Ramaswamy (2011), A model investigation of aerosol-induced changes in tropical circulation, *J. Clim.*, *24*, 5125–5133.

Ming, Y., V. Ramaswamy, L. J. Donner, and V. T. J. Phillips (2006), A new parameterization of cloud droplet activation applicable to general circulation models, *J. Atmos. Sci.*, *63*, 1348–1356, doi:10.1175/JAS3686.1.

Ming, Y., V. Ramaswamy, L. J. Donner, V. T. J. Phillips, S. A. Klein, P. Ginoux, and L. W. Horowitz (2007), Modeling the interaction between aerosols and liquid water clouds with a self-consistent cloud scheme in a general circulation model, *J. Atmos. Sci.*, *64*, 1189–1209, doi:10.1175/JAS3874.1.

Po-Chedley, S., and Q. Fu (2012), Discrepancies in tropical upper tropospheric warming between atmospheric circulation models and satellites, *Environ. Res. Lett.*, *7*, 044018, doi:10.1088/1748-9326/7/4/044018.

Polvani, L. M., D. W. Waugh, G. J. P. Correa, and S. W. Son (2011), Stratospheric ozone depletion: the main driver of twentieth-century atmospheric circulation changes in the Southern Hemisphere, *J. Clim.*, *24*, 795–812, doi:10.1175/2010JCLI3772.1.

Ramaswamy, V., J. W. Hurrell, and G. A. Meehl (2006), Why do temperature vary vertically (from the surface to the stratosphere) and what do we understand about why they might vary and change over time?, in *Temperature Trends in the lower atmosphere: steps for understanding and reconciling differences*, edited by T. R. Karl, S. J. Hassol, C. D. Miller, and W. L. Murray, Washington, DC.

Randel, W. J., and I. M. Held (1991), Phase speed spectra of transient eddy fluxes and critical layer absorption, *J. Atmos. Sci.*, *48*, 6888–6897.

Randel, W. J., and E. J. Jensen (2013), Physical processes in the tropical tropopause layer and their roles in a changing climate, *Nat. Geosci.*, *6*, 169–176.

Randel, W. J., and F. Wu (1996), Isolation of the ozone QBO in SAGE II data by singular-value decomposition, *J. Atmos. Sci.*, *53*, 2546–2559.

Randel, W. J., R. R. Garcia, N. Calvo, and D. Marsh (2009), ENSO influence on zonal mean temperature and ozone in the tropical lower stratosphere, *Geophys. Res. Lett.*, *36*, L15822, doi:10.1029/2009GL039343.

Robock, A. (2000), Volcanic eruptions and climate, *Rev. Geophys.*, *38*, 191–219.

Rosenlof, K. H. (1995), Seasonal cycle of the residual mean meridional circulation in the stratosphere, *J. Geophys. Res.*, *100*, 5173–5191, doi:10.1029/94JD03122.

Santee, M. L., and D. Crisp (1995), Diagnostic calculations of the circulation in the Martian atmosphere, *J. Geophys. Res.*, *100*, 5465–5484.

Seager, R., N. Harnik, Y. Kushnir, W. Robinson, and J. Miller (2003), Mechanisms of hemispherically symmetric climate variability, *J. Clim.*, *16*, 2960–2978.

Seviour, W. J. M., N. Butchart, and S. C. Hardiman (2012), The Brewer-Dobson circulation inferred from ERA-Interim, *Q. J. Roy. Meteorol. Soc.*, *138*, 878–888, doi: 10.1002/qj.966.

Shepherd, T. G., and C. McLandress (2011), A robust mechanism for strengthening of the Brewer-Dobson circulation in response to climate change: critical-layer control of subtropical wave breaking, *J. Atmos. Sci.*, *68*, 784–797, doi:10.1175/2010JAS3608.1.

Simpson, I. R., T. G. Shepherd, and M. Sigmond (2011), Dynamics of the lower stratospheric circulation response to ENSO, *J. Atmos. Sci.*, *68*, 2537–2556.

Solomon, S., J. T. Kiehl, R. R. Garcia, and W. Grose (1986), Tracer transport by the diabatic circulation deduced from satellite observations, *J. Atmos. Sci.*, *43*, 1603–1617.

Solomon, S., K. H. Rosenlof, P. W. Robert, J. S. Daniel, S. M. Davis, T. J. Sanford, and G. K. Plattner (2010), Contribution of stratospheric water vapor to decadal changes in the rate of global warming, *Science*, *327*, 1219–1223.

SPARC CCMVal (2010), Chemistry-Climate Model validation, SPARC Report No. 5, WCRP-30, WMO/TD-No. 40, http://www.sparc-climate.org/publications/sparc-reports/sparc-report-no5/.

Taylor, K. E., R. J. Stouffer, and G. A. Meehl (2012), An overview of CMIP5 and the experiment design, *Bull. Am. Meteor. Soc.*, *93*, 485–498.

Thompson, D. W. J., M. P. Baldwin, and J. M. Wallace (2002), Stratospheric connection to Northern Hemispher wintertime weather: implications for prediction, *J. Clim.*, *15*, 1421–1428.

Tilmes, S., R. R. Garcia, D. E. Kinnison, A. Gettelman, and P. J. Rasch (2009), Impact of geoengineered aerosols on the troposphere and stratosphere, *J. Geophys. Res.*, *114*, D12305, doi:10.1029/2008JD011420.

Trenberth, K. E., and D. P. Stepaniak (2001), Indices of El Niño evolution, *J. Clim.*, *14*, 1697–1701.

von Storch, H., and F. W. Zwiers (1999), *Statistical Analysis in Climate Research*, 484 pp., Cambridge University Press, New York.

WMO (2011), Scientific assessment of ozone depletion: 2010, *Global Ozone Research and Monitoring Project-Report 52*, Geneva, Switzerland.

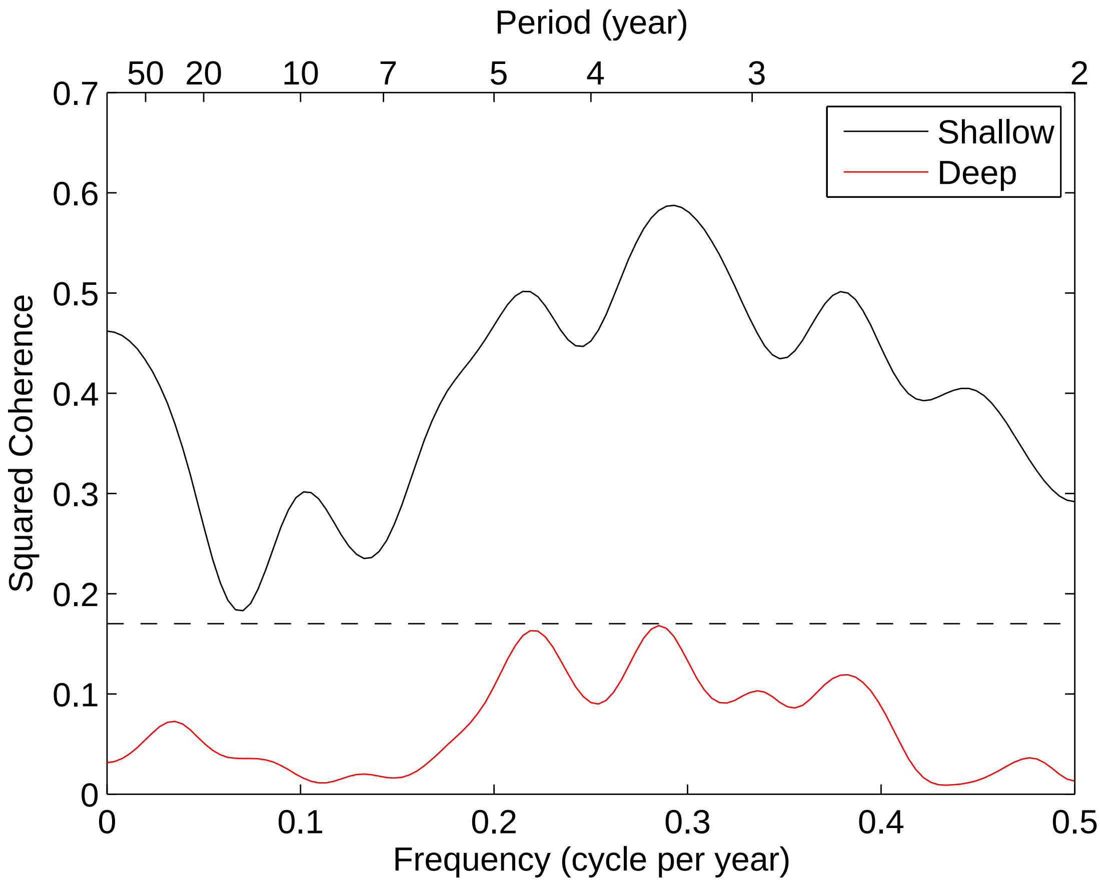

Figure 1. Squared coherence between the strength of the Brewer-Dobson circulation and the tropical-mean surface temperature. The black line is for the shallow branch of the Brewer-Dobson circulation, and the red line for the deep branch. The dashed line marks the critical value for the 95% significance level test of zero coherency. Results are based on the 1700-year pre-industrial control simulation. See appendix for details of the cross-spectrum calculation.

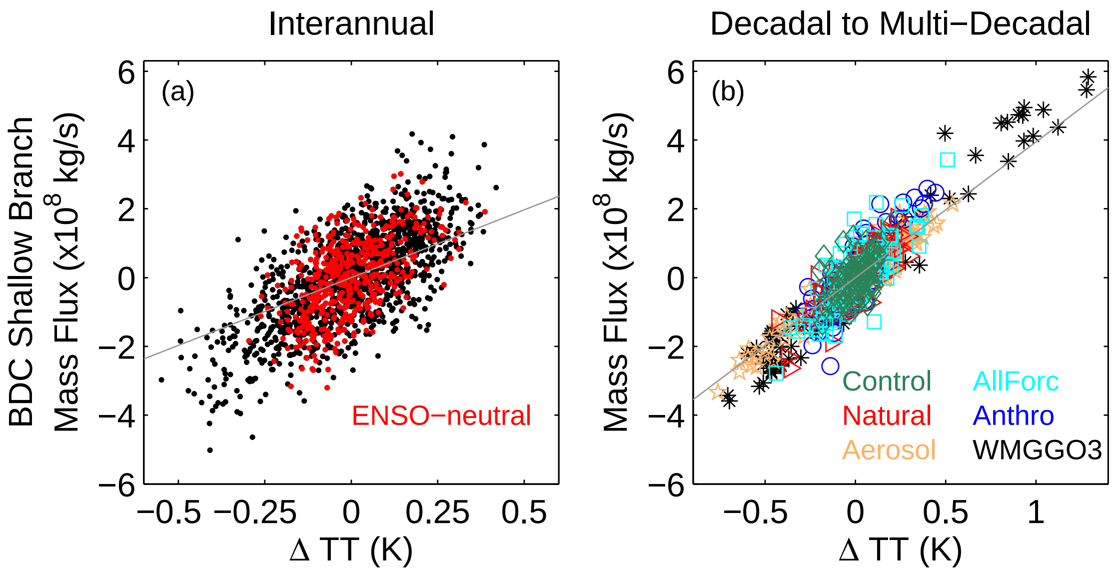

Figure 2. Scatter plot of the strength of the Brewer-Dobson circulation shallow branch versus the tropical-mean surface temperature in CM3. (a) For the interannual timescale in the control simulation. ENSO-neutral years are marked by red dots. (b) For the decadal to multi-decadal timescale in the control and historical forced simulations. Climatological means are removed. The gray line marks the result from the an idealized experiment in which SST is globally uniformly increased by 4K.

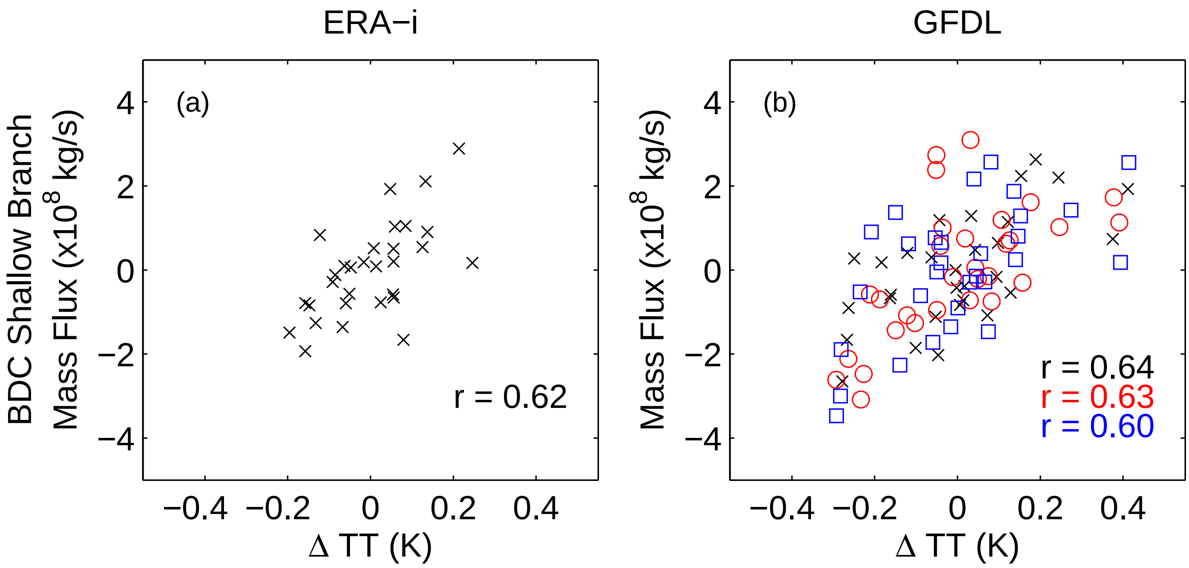

Figure 3. Scatter plot of the strength of the Brewer-Dobson circulation shallow branch versus tropical-mean surface temperature (a) from the ERA interim reanalysis for 1981-2010, and (b) from the three-member ensemble of AM3 AllForc simulation for 1974-2003. Only the interannual timescale is considered here. Correlation coefficients are given in the lower-right corner of each panel. Note that the QBO-related signals are removed from the reanalysis data.

Table 1. Correlation Coefficients between the strength of the Brewer-Dobson circulation and the tropical-mean surface temperature. Correlations are calculated for variations on the interannual and the decadal to multi-decadal timescales (See text for definitions). For the interannual timescale, correlations are also calculated using a subset of ENSO-neutral years with results shown in parentheses. Correlations that are not statistical significantly different from zero at the 99% confidence level are underlined. Red noises in time series are taken into account. Note that the QBO-related signals are removed from the reanalysis data.

		Shallow branch		Deep branch	
		Interannual	Decadal to Multi-decadal	Interannual	Decadal to Multi-decadal
ERA-i		0.62	-	$\underline{-0.26}$	-
AM3	AllForc	0.64	-	0.57	-
		0.63	-	$\underline{0.23}$	-
		0.60	-	$\underline{0.30}$	-
CM3	Control	0.68 (0.56)	0.59	0.27 (0.25)	$\underline{0.18}$
	AllForc	0.75 (0.59)	0.80	0.23 (0.29)	0.49
	Natural	0.67 (0.46)	0.83	0.31 ($\underline{0.24}$)	$\underline{0.36}$
	Anthro	0.66 (0.49)	0.86	0.34 (0.31)	0.73
	Aerosol	0.67 (0.50)	0.96	0.31 ($\underline{0.25}$)	$\underline{0.58}$
	WMGGO3	0.67 (0.59)	0.98	0.22 ($\underline{0.18}$)	$\underline{0.90}$
CM2.1	Natural	0.75 (0.66)	0.70	0.48 (0.43)	$\underline{0.09}$
	Aerosol	0.71 (0.67)	0.60	0.60 (0.69)	$\underline{0.31}$
	WMGGO3	0.78 (0.54)	0.95	0.64 (0.42)	0.91

Tropical Climate Change Control of the Lower Stratospheric Circulation: Supplementary Materials

Pu Lin

Program in Atmospheric and Oceanic Sciences, Princeton University.[*]

Yi Ming and V. Ramaswamy

Geophysical Fluid Dynamics Laboratory / NOAA

(Dated: December 9, 2014)

[*] To whome correspondence should be addressed:

Pu.Lin@noaa.gov

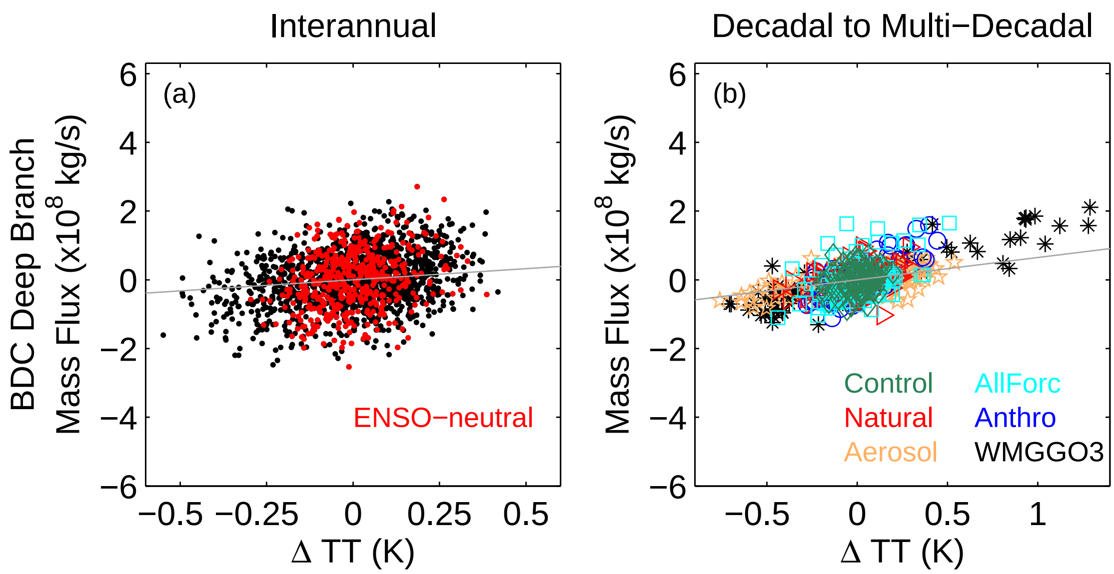

Figure S1. Scatter plot of the Brewer-Dobson deep branch versus the tropical-mean surface temperature in CM3. (a) For the interannual anomalies in the control simulations. ENSO-neutral years are maked by read dots. (b) For the multi-decadal timescale in the control and historical forced simulations. Climatological means are removed. The gray line marks the result from the an idealized experiment in which SST is globally uniformly increased by 4K.

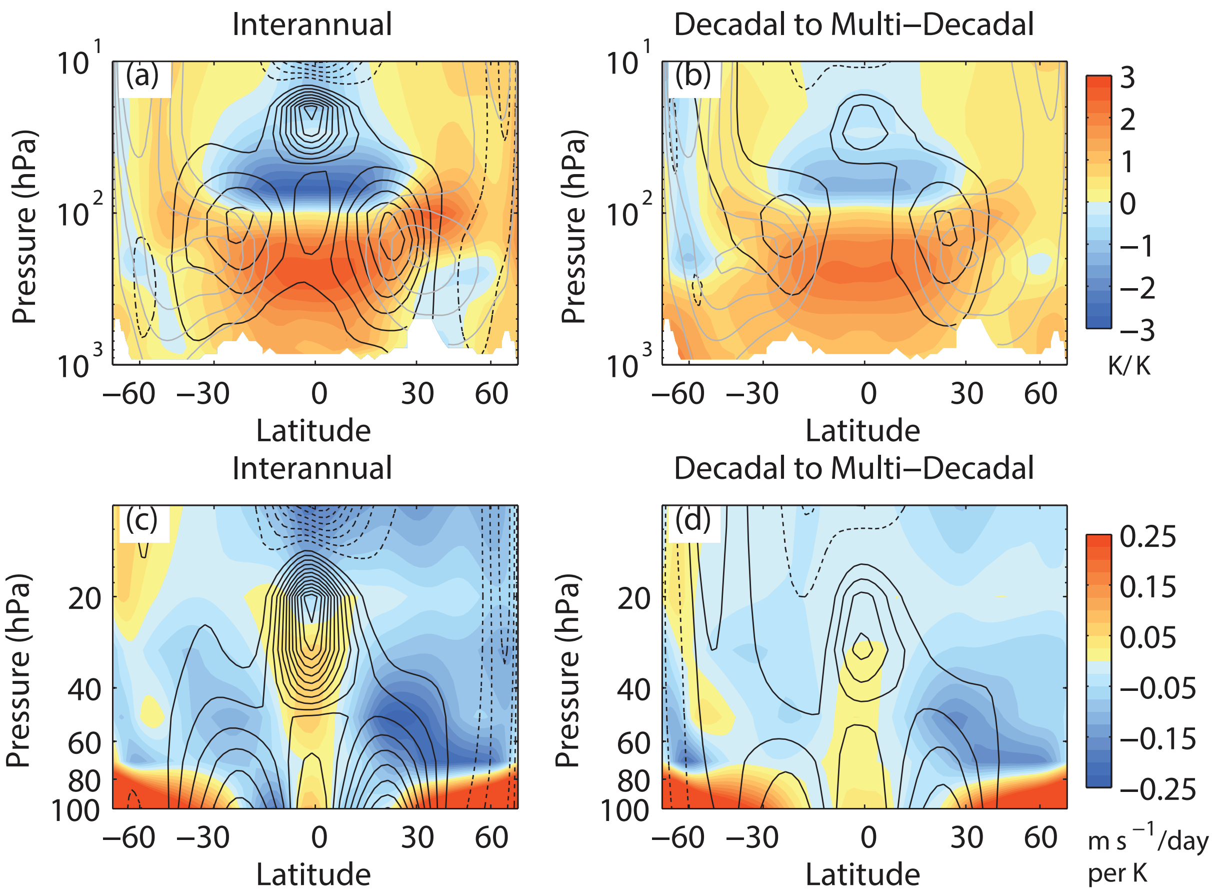

Figure S2. Response in zonal mean temperature, zonal wind and wave forcing to changes in the tropical mean surface temperature. (a) and (b) Regression of zonal mean temperature (color shading) and zonal wind (black contours) upon tropical mean surface temperature from the control simulation. Contour interval for zonal wind regression is 1.5 m/s/K, with negative contours in dashed lines, and the zero contour is omitted. The climatology of zonal mean zonal wind (light gray contours) is also plotted for comparison. Contour interval for zonal wind climatology is 7.5 m/s. Zero wind and easterlies are omitted for clarity. (c) and (d) Regression of zonal mean zonal wind (contours) and wave forcing (color shading) upon the tropical mean surface temperature from the control simulation. See Appendix A for the definition of the wave forcing. Contour interval for zonal wind regression is 1 m/s/K, with negative contours in dashed lines and the zero contour is omitted. (a) and (c) are for the interannual timescale, and (b) and (d) for the decal to multi-decadal timescale. Note that the strong signals in the wind regression near the equator are not statistically significant.

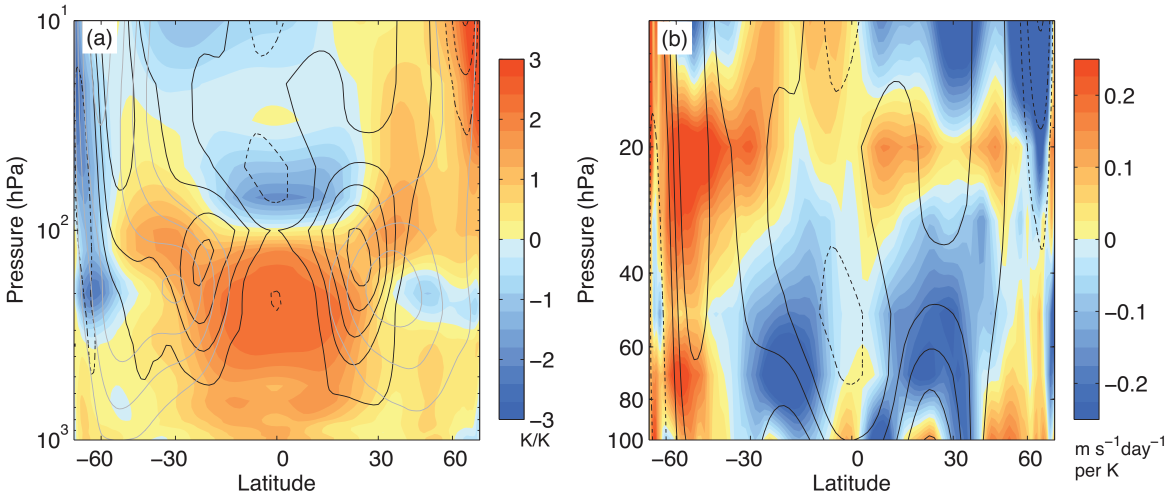

Figure S3. Response to changes in tropical mean surface temperature on the interannual timescale in the ERA-interim reanalysis for 1981-2010. (a) Regression of zonal mean temperature (color shading) and zonal wind (black contours) upon the tropical mean surface temperature. Contour interval for zonal wind regression is 1.5 m/s/K, with negative contours in dashed lines, and the zero contour is omitted. Zonal mean zonal wind climatology is plotted in gray contours for comparison. Contour interval for zonal wind climatology is 7.5 m/s, and only westerlies are plotted for clarity. (b) Regression of zonal mean zonal wind (contours) and wave forcing (color shading) upon the tropical mean surface temperature. Contour interval is 1.5 m/s/K, with negative contours in dashed lines, and the zero contour is omitted. The QBO signals are removed before the regression.

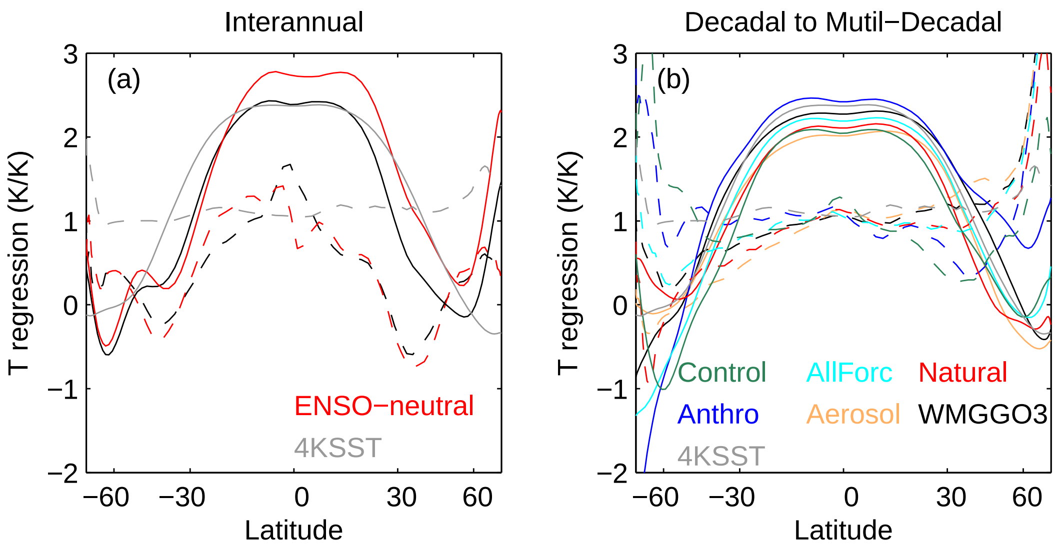

Figure S4. Regression of temperature at surface (dashed lines) and at 200 hPa (solid lines) upon TT. (a) For variations on the interannual timescale, the results using ENSO-neutral years are in red. (b) For variations on the decadal to multi-decadal timescale, results from simulations with different forcings are plotted in different colors. For comparison, the temperature changes at the surface and the 200 hPa level (normalized by the tropical surface temperature change) from the idealized 4KSST experiment is also plotted in gray.

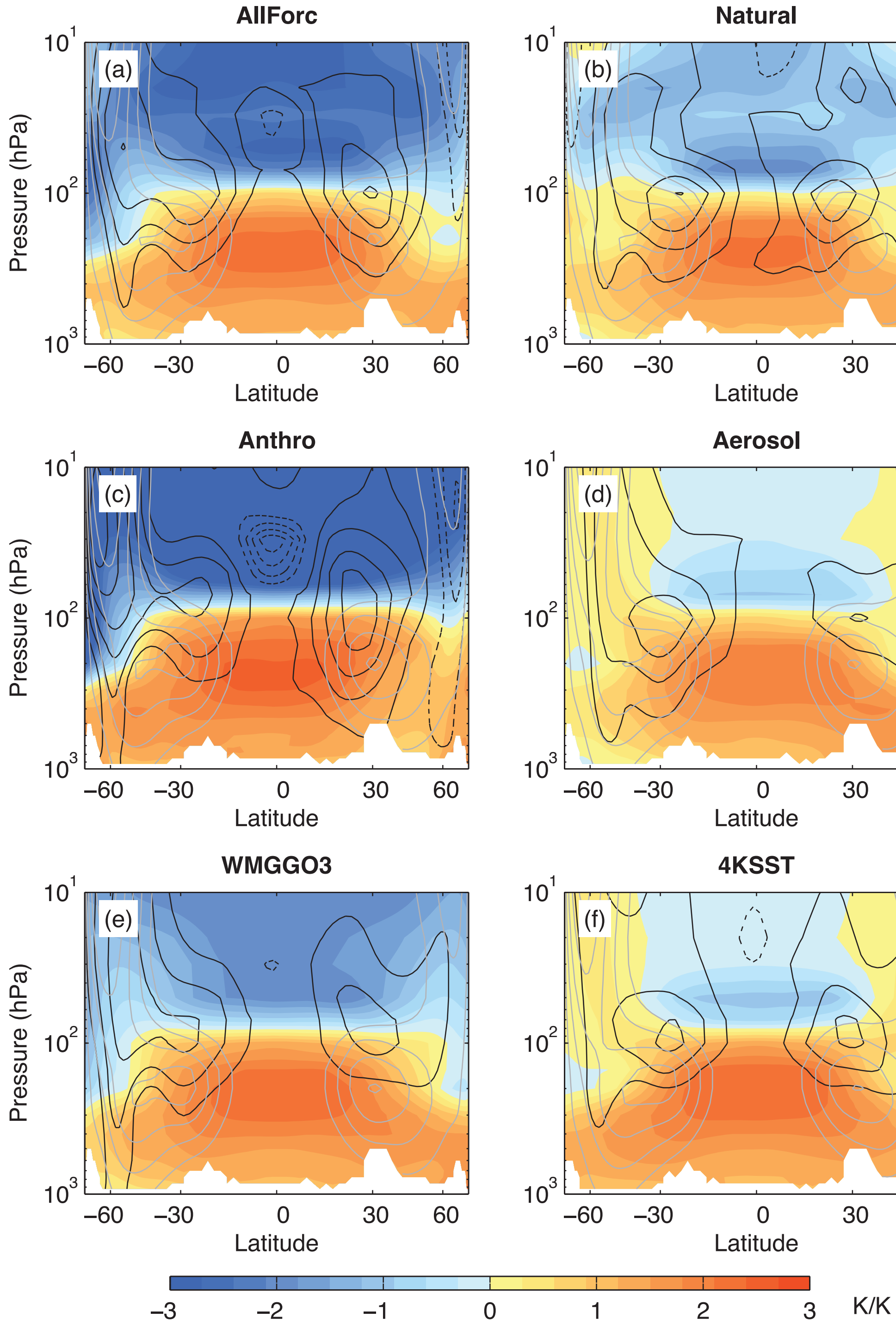

Figure S5. Regression of zonal mean temperature (color shading) and zonal wind (black contours) upon tropical mean surface temperature on the decadal to multi-decadal timescale from the historical simulations with (a) all forcings, (b) natural forcings, (c) anthropogenic forcings, (d) anthropogenic aerosol forcings, and (e) GHGs and ozone forcings. (f) Zonal mean temperature and zonal wind changes per unit surface temperature change from the idealized 4KSST experiment. Contour interval for zonal wind regression is 0.75 m/s/K, with negative contours in dashed lines, and the zero contour is omitted. Zonal mean zonal wind climatology is plotted in gray contours for comparison. Contour interval for zonal wind climatology is 7.5 m/s, and only westerlies are plotted for clarity.

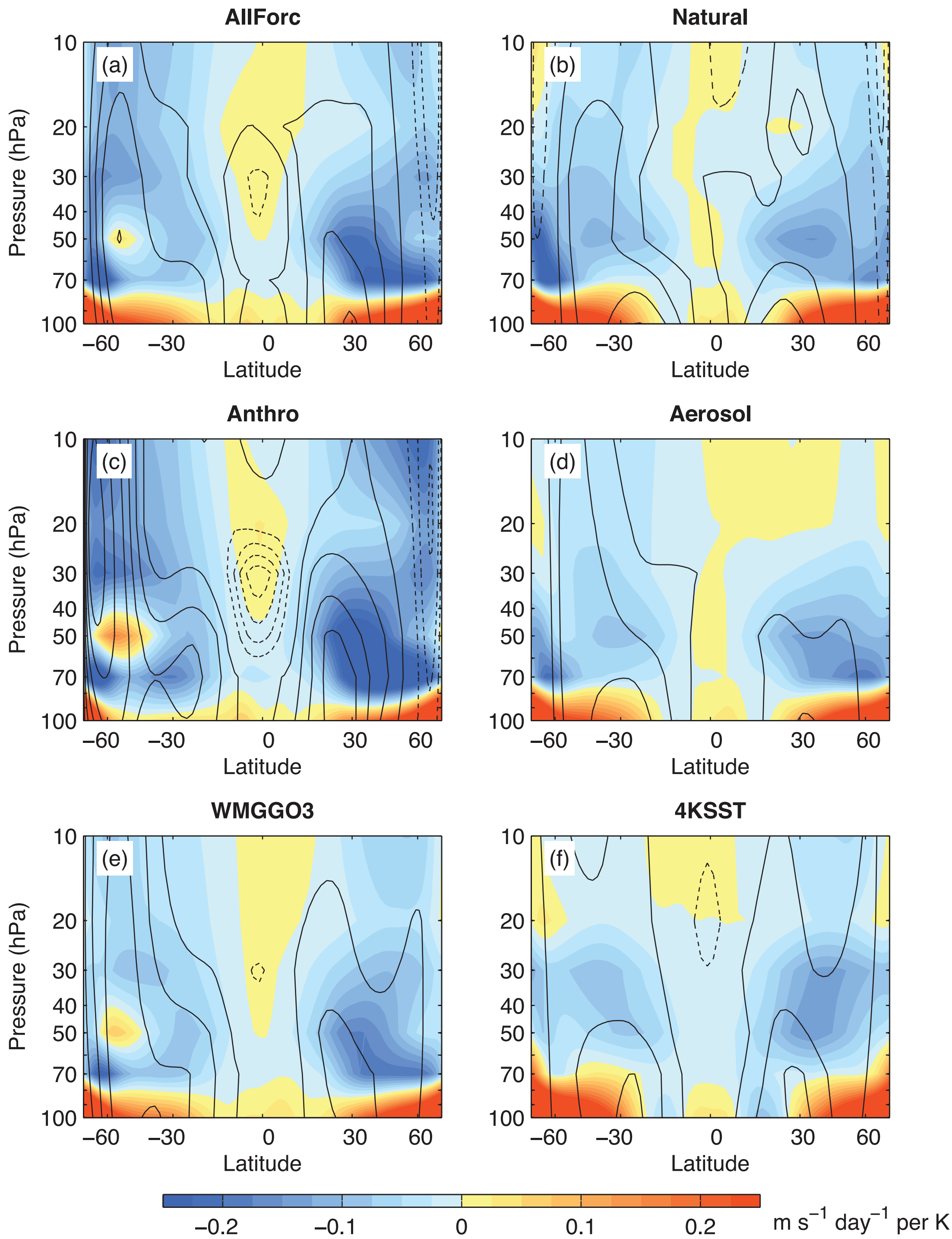

Figure S6. As in Fig. S5 except for wave forcing X (color shading) and the zonal mean zonal wind (contours). Contour interval for zonal wind regression is 0.75 m/s/K, with negative contours in dashed lines, and the zero contour is omitted. See Appendix A for the definition of the wave forcing.